AD-A072 829 TRW DEFENSE AND SPACE SYSTEMS GROUP REDONDO BEACH CA F/G 17/1
FIBER OPTIC DETECTION OF LOW FREQUENCY UNDERWATER SOUND.(U)
JUN 79 D W BAGGETT, R L JOHNSON N00014-76-C-0490
UNCLASSIFIED TRW-AT-ATD-TR-79-2 NL

| OF |
AD
A072829

END
DATE
FILMED
9-79
DDC

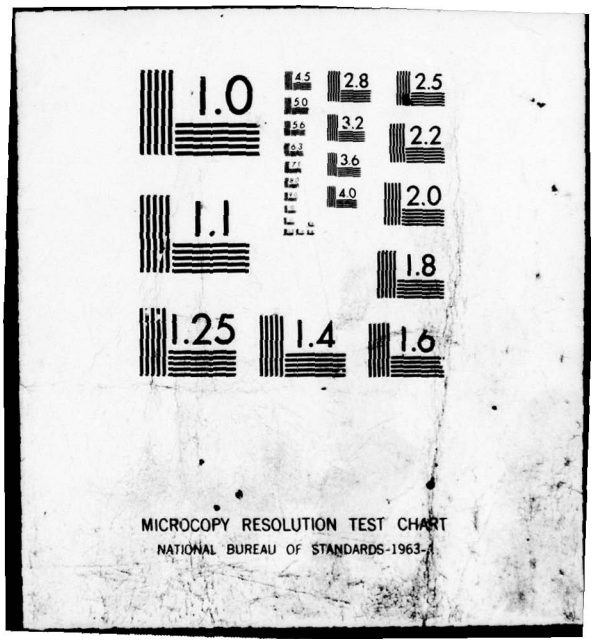
1.0
1.1
1.25
1.4
1.6
1.8
2.0
2.2
2.5
2.8
3.2
3.6
4.0
4.5
5.0
5.6
6.3
MICROCOPY RESOLUTION TEST CHART
NATIONAL BUREAU OF STANDARDS-1963-A

AD A072829

LEVEL II

DDC
RECEIVED
AUG 16 1979
C

FIBER OPTIC DETECTION OF LOW FREQUENCY UNDERWATER SOUND

FINAL REPORT

AT-ATD-TR-79-2

28 June 1979

DDC FILE COPY

Sponsored by

Office of Naval Research
Contract No. N00014-76-C-0490
Task No. NR089-117
Code 465

APPROVED FOR PUBLIC RELEASE; DISTRIBUTION UNLIMITED

TRW
DEFENSE AND SPACE SYSTEMS GROUP
One Space Park
Redondo Beach, California 90278

79 08 16 039

FIBER OPTIC DETECTION
OF LOW FREQUENCY UNDERWATER SOUND

FINAL REPORT

AT-ATD-TR-79-2

28 June 1979

Sponsored by

Office of Naval Research
Contract No. N00014-76-C-0490
Task No. NR089-117
Code 465

APPROVED FOR PUBLIC RELEASE; DISTRIBUTION UNLIMITED

TRW
DEFENSE AND SPACE SYSTEMS GROUP
One Space Park
Redondo Beach, California 90278

UNCLASSIFIED

SECURITY CLASSIFICATION OF THIS PAGE (When Data Entered)

REPORT DOCUMENTATION PAGE		READ INSTRUCTIONS BEFORE COMPLETING FORM
1. REPORT NUMBER	2. GOVT ACCESSION NO.	3. RECIPIENT'S CATALOG NUMBER
4. TITLE (and Subtitle) (6) FIBER OPTIC DETECTION OF LOW FREQUENCY UNDERWATER SOUND,		5. TYPE OF REPORT & PERIOD COVERED Final 4/01/76-4/30/79
		6. PERFORMING ORG. REPORT NUMBER (14) TRW-AT-ATD-TR-79-2
7. AUTHOR(s) (10) D. W. Baggett and R. L. Johnson		8. CONTRACT OR GRANT NUMBER(s) N00014-76-C-0490 (15)
9. PERFORMING ORGANIZATION NAME AND ADDRESS TRW Defense and Space Systems Group One Space Park Redondo Beach, California 90278		10. PROGRAM ELEMENT, PROJECT, TASK AREA & WORK UNIT NUMBERS NR 089-117
11. CONTROLLING OFFICE NAME AND ADDRESS Office of Naval Research 800 N. Quincy St. Arlington, VA 22217 (12) 32p. (11)		12. REPORT DATE 28 June 1979
		13. NUMBER OF PAGES 31
14. MONITORING AGENCY NAME & ADDRESS (if different from Controlling Office)		15. SECURITY CLASS. (of this report) UNCLASSIFIED
		15a. DECLASSIFICATION DOWNGRADING SCHEDULE

16. DISTRIBUTION STATEMENT (of this Report)

Approved for public release; distribution is unlimited.

17. DISTRIBUTION STATEMENT (of the abstract entered in Block 20, if different from Report)

(9) Final rept. 4 Jan 76-31 Apr 79

18. SUPPLEMENTARY NOTES

R. Gracen Joiner
ONR Scientific Officer

19. KEY WORDS (Continue on reverse side if necessary and identify by block number)

Acoustic Detection
Acousto-Optic
Fiber Optics
Interferometer
Sonar

20. ABSTRACT (Continue on reverse side if necessary and identify by block number)

Theoretical and experimental studies of acousto-optic interferometry were continued. An experimental test of the differential loop interferometer demonstrated that the theoretical sensitivity limit can be achieved with acoustic frequencies from 1 kHz to 50 kHz. The Michelson interferometer was studied under an environmentally stabilized configuration, but the theoretical sensitivity limit was not achieved. A Fabry-Perot configuration was analyzed, giving a theoretical prediction of very high sensitivity per unit fiber length.

DD FORM 1 JAN 73 1473 EDITION OF 1 NOV 65 IS OBSOLETE

UNCLASSIFIED

SECURITY CLASSIFICATION OF THIS PAGE (When Data Entered)

409 637

PREFACE

This report was prepared by TRW Defense and Space Systems Group, Redondo Beach, California, under Contract N00014-76-C-0490 with the Office of Naval Research, Arlington, Virginia. The authors wish to acknowledge the technical assistance of Mr. H. E. Hunley.

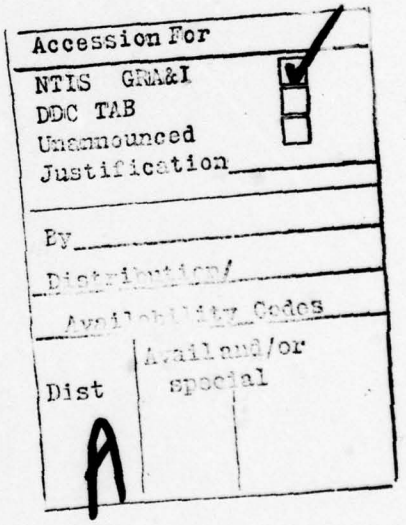

TABLE OF CONTENTS

1.0 INTRODUCTION

Optical detection of underwater sound has great potential for naval sonar applications. This report contains an analysis of several types of acousto-optic interferometers, comparisons between the interferometers, and the results of experimental efforts aimed at verifying the theoretical analysis.

Acousto-optic interferometry is performed by phase modulating a beam of light with the acoustic field that is to be detected, and observing this phase modulation by optical interferometry. The major advantage of this technique is found with the use of optical fibers. An optical fiber immersed in water will carry light long distances with low loss, so that the interferometer can use long path lengths. The index of refraction of the fiber is modulated by acoustic pressure by an amount directly proportional to the peak pressure. Thus, an acousto-optic interferometer can be made very sensitive by using long fibers.

The major objectives of this research program were to analyze and compare several potential phase-detecting interferometers, and to experimentally test the feasibility of their use in sonar arrays. The Michelson, Sagnac, and Fabry-Perot interferometers were analyzed, and their advantages and disadvantages as sound transducers were evaluated. It was determined that the Michelson interferometer is potentially the most sensitive, if noise resulting from the separate reference and sensing legs can be overcome. A possible approach towards reducing this noise by environmentally coupling the reference and sensing legs was examined. The Sagnac (loop) interferometer was experimentally tested. The theoretical noise advantages were verified since the detector shot noise was found to be the limiting factor.

2.0 ANALYSIS

2.1 THE DIFFERENTIAL INTERFEROMETER

The differential interferometer is a version of the Sagnac interferometer, in which light is sent in both directions around a loop using a beam splitter. A portion of the loop passes through an acoustic field, while the other portion of the loop is isolated from the acoustic field (see Figure 1).

Both beams of light (one traveling in each direction) are modulated by the sound waves, as the sound waves modulate the index of refraction of the transmitting media. For our purposes, the transmitting media is either water or an optical fiber immersed in water. Each beam of light senses the acoustic field at a different time. This is because one beam enters the acoustic field immediately after leaving the beam splitter, while the other must first propagate around the time-delay path. Thus, each beam experiences a slightly different phase shift due to the fact that the acoustic pressure changes during the propagation time through the delay leg. This causes the two-beam interference pattern at the detector to be modulated by an amount proportional to the time derivative of the acoustic wave and proportional to the delay time introduced by the delay leg.

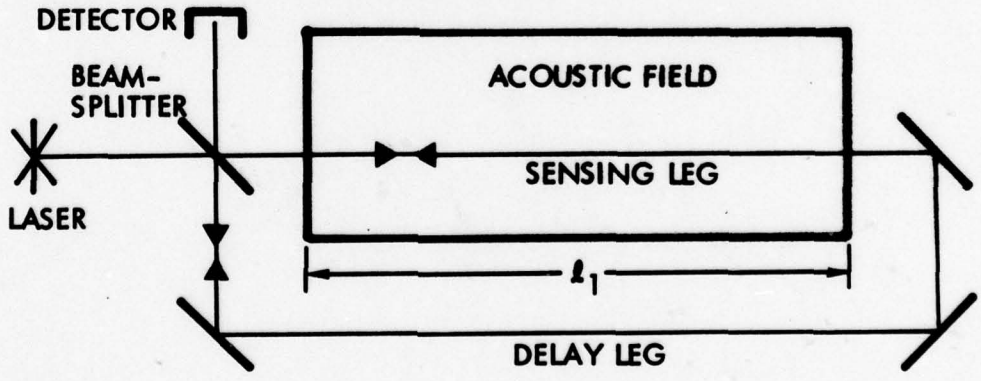

Figure 1. The differential interferometer

The advantage of the differential interferometer over the more traditional Michelson interferometer is the optical stability that can be gained if the differential interferometer is constructed properly. Consider the two-mirror setup shown in Figure 2. Initially it is aligned so that both beams fall on the same point at the detector surface (Fig. 2a). Now suppose that one of the mirrors is vibrating. If it rotates through an angle α, the reflected beam will rotate through an angle 2α, and will be shifted on the detector surface as shown in Figures 2b,c. Note that both beams are shifted in the same direction (although not quite the same amount). This reduces the disturbance of the interference pattern by vibrations. However, if there are three mirrors (or more generally an odd number of mirrors) in the configuration, a rotation of one mirror will cause the beams to shift in opposite directions, defeating the purpose of the differential interferometer (see Figure 3).

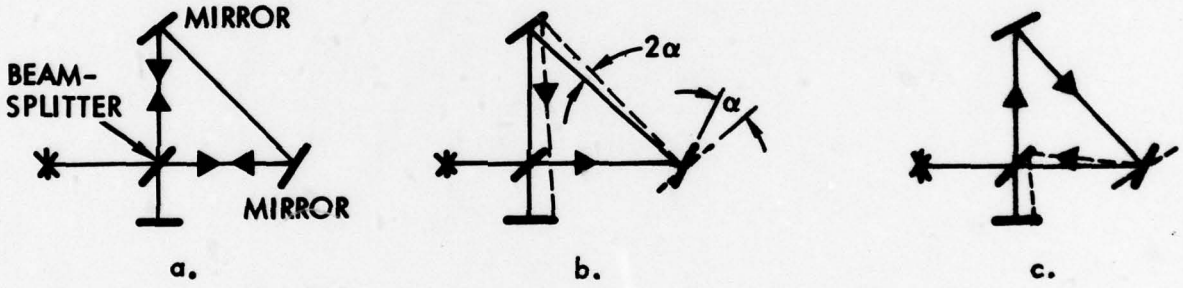

Figure 2. Vibrational stability of the differential interferometer with an even number of mirrors.

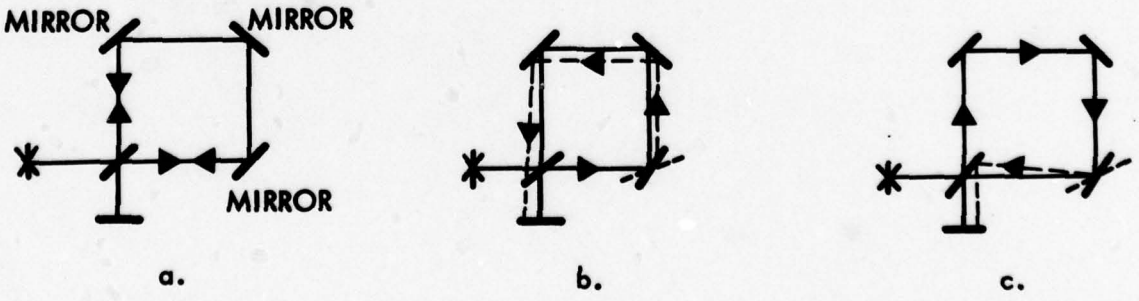

Figure 3. Vibrational instability of the differential interferometer with an odd number of mirrors.

The light power at the detector of the differential interferometer can be calculated in the same manner as with any two-beam interferometer. We assume that the beam-splitter divides the incident laser beam into two beams of equal amplitude. After traversing the loop, the magnitudes of the electric field vectors of each of the beams are given by

$$E_1 = A\, e^{i(kx-\omega t)+i\phi_1}$$

$$E_2 = A\, e^{i(kx-\omega t)+i\phi_2}$$

The power of the combined beams is given by the magnitude of the square of the sum of the electric field vectors, which is easily shown to be

$$P_d = 2\, A^2[1 + \cos(\phi_2 - \phi_1)] \qquad (1)$$

This expression is valid for any two-beam interferometer which preserves the polarization of the beams. However, the phase difference $\phi_2 - \phi_1$ depends upon the specific type of interferometer used. As we will see, this phase difference must be set carefully to provide a maximum modulation of the intensity on the detector.

For the differential interferometer the phase shift of each beam can be calculated from the expression

$$d\phi = k\, \Delta n\, d\ell$$

where $d\ell$ is distance along the laser beam, k is the optical wave number, and Δn is the change in index of refraction of the transmitting media induced by the sound waves. This change is given by

$$\Delta n = \frac{\partial n}{\partial p}\, \Delta p = \frac{\partial n}{\partial p}\, p_o \cos(K_x x - \Omega t)$$

where p_o is the peak acoustic pressure, Ω is the acoustic frequency, and K_x is the component of the acoustic wave number in the direction of light propagation. For a plane acoustic wave crossing the light beam at angle θ, we get the expression $K_x = K\sin\theta$.

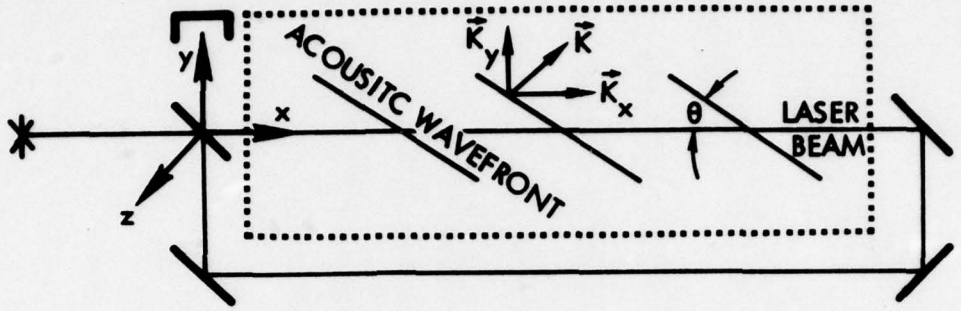

Figure 4. Coordinate system for differential interferometer

We calculate the phase shift of each beam by assuming that the light senses the acoustic field instantaneously and then integrating over the spatial dimension of the acoustic field. This gives the expressions

$$\phi_1 = k \frac{\partial n}{\partial p} p_o \int_o^{\ell_1} \cos(K_x x - \Omega t_1) dx$$

$$\phi_2 = k \frac{\partial n}{\partial p} p_o \int_o^{\ell_1} \cos(K_x x - \Omega t_2) dx$$

where $t_2 - t_1$ is the delay time given by

$$t_2 - t_1 = \frac{\ell_2}{c}$$

where ℓ_2 is the length of the delay leg and c is the speed of light in the medium of the delay leg. If we integrate and simplify the preceding expressions for ϕ_1 and ϕ_2, we get

$$\phi_2 - \phi_1 \cong k \frac{\partial n}{\partial p} p_o \frac{\sin \frac{K_x \ell_1}{2}}{\frac{K_x \ell_1}{2}} \frac{\Omega}{c} \ell_1 \ell_2 \sin(\Omega t_2 - \frac{K_x \ell_1}{2})$$

In deriving this expression we have used the approximations

$$\sin \frac{\Omega \ell_2}{c} \cong \frac{\Omega \ell_2}{c}$$

$$\cos \frac{\Omega \ell_2}{c} \cong 1 - \frac{\Omega^2 \ell_2^2}{2c^2}$$

The change in index of refraction with pressure can be expressed using the Lorentz-Lorenz equation as

$$\frac{\partial n}{\partial p} = \frac{\partial n}{\partial \rho}\frac{\partial \rho}{\partial p}\bigg|_s \cong \frac{n-1}{\rho c_s^2}$$

where c_s is the speed of sound.

If the acoustic field is propagating in a direction normal to the beam direction, the phase shift seen at the detector is given by

$$\Delta\phi = \phi_2 - \phi_1$$

$$\cong k \frac{n-1}{\rho c_s^2} p_o \frac{\Omega}{c} \ell_1 \ell_2 \sin\Omega t \qquad (2)$$

Referring back to Eq. 1, we see that the a.c. component of power incident on the detector is proportional to $\cos\Delta\phi$. Since $\Delta\phi$ is small (10^{-6} rad),

$$\cos\Delta\phi \cong 1 - \frac{\Delta\phi^2}{2}$$

This is a very good approximation. This means that we must detect the square of a very small phase shift, assuming the interferometer is aligned so that there is no phase difference between the two beams except that introduced by the sound waves. However, if we insert a $\pi/2$ phase shift into one beam, the a.c. component of power on the detector is proportional to $\cos(\Delta\phi - \pi/2) = \sin\Delta\phi$. We can now use the approximation $\sin\Delta\phi \cong \Delta\phi$. Thus, with a $\pi/2$ phase difference between the beams, the detector will respond to $\Delta\phi$ rather than the square of $\Delta\phi$, meaning that the sensitivity will be greatly enhanced. With this phase shift, Eq. 1 can be written as

$$P_d = \frac{P_o}{2}(1 + \Delta\phi)$$

where $P_o = (2A)^2$ is the laser power.

This phase difference can be introduced by aligning the two beams along slightly different axes, so that the wavefronts are not parallel. This will produce fringes across the area of overlap of the two beams. The light at the edges of the fringes will experience the greatest modulation as $\Delta\phi$ changes, so the detector should be placed there. If the detector area is roughly equal to the cross-sectional area of the laser beam, the interferometer should be aligned so that one fringe falls across the detector face.

Another method of introducing this phase shift was suggested earlier[1] but has proven to be difficult to accomplish and also unnecessary. The idea was to frequency shift one of the beams by using a Bragg cell. This effectively sweeps the phase difference between the beams, so that part of the time the system is set at maximum sensitivity, regardless of the angle between the optical wavefronts (within reason). One difficulty is that the detector must be able to respond to the frequency difference between the beams, which is necessarily near 40 MHz. Another difficulty is the optical loss associated with the Bragg cell.

Ideally, the interferometer should be limited by the fundamental detector noise, either shot noise or thermal noise. In practice this is not always the case. Vibrations of the optical components, laser fluctuations, and electromagnetic interference can all reduce the sensitivity of the interferometer. By calculating the shot noise limited sensitivity and thermal noise limited sensitivity, we can determine whether the experimental results are limited by the fundamental noise or by other factors.

Shot noise is caused by current fluctuations across the diode junction, and is given by

$$i_N = \sqrt{2e\Delta F i}$$

where e is the electronic charge, ΔF is the bandwidth of the measuring instrument, and i is the current through the diode. Since each photon that is absorbed by the diode creates an electron-hole pair, the photocurrent through the diode is given by

$$i = \eta e \frac{dN}{dt} = \eta e \frac{P_d}{h\nu} \tag{3}$$

where η is the quantum efficiency of the detector, dN/dt is the number of photons falling on the detector surface per unit time, P_d is the incident light power on the detector, h is Planck's constant, and ν is the frequency of the light. The power signal to noise ratio is given by

$$SNR = \frac{\langle i_{ac}^2 \rangle}{\langle i_N^2 \rangle}$$

where i_{ac} is the a.c. component of the diode current and where the brackets indicate time average. The power at the detector is given by $P_d = P_o(1+\Delta\phi)/2$, where $P_o\Delta\phi/2$ is the a.c. component. Using this, we get

$$SNR = \frac{\eta P_o}{4h\nu\Delta F} \langle \Delta\phi^2 \rangle$$

By using the expression for $\Delta\phi$ found in Eq. 2 and assuming that the lowest signal to noise ratio we can use and still detect the signal is SNR = 1, we can solve for the minimum detectable acoustic pressure, limited by shot noise. We get

$$P_{o,shot} = \frac{\lambda_o c \rho c_s^2}{\pi\Omega\ell_1\ell_2(n-1)} \sqrt{\frac{2h\nu\Delta F}{\eta P_o}} \tag{4}$$

Thermal noise is caused by thermal agitation of charge carriers in a resistor. The noise power is given by

$$P_N = 4\ k\ T\Delta F$$

where k is Boltzmann's constant and T is the temperature in degrees Kelvin. The power signal to noise ratio is given by

$$SNR = \frac{\langle i_{ac}^2 \rangle R}{P_N} = \frac{\left(\frac{\eta e P_o}{2h\nu}\right)^2 \langle \Delta\phi^2 \rangle R}{4k\ T\ \Delta F}$$

where R is the load resistance across the detector. Using Eq. 2 to express $\Delta\phi$, setting SNR = 1, and solving for the peak acoustic pressure gives the minimum detectable pressure which is limited by thermal noise. Thus,

$$p_{o,thermal} = \frac{\lambda_o c \rho c_s^2}{\pi \Omega \ell_1 \ell_2 (n-1)} \frac{h\nu}{\eta e P_o} \sqrt{\frac{3kT\Delta F}{R}} \tag{5}$$

The theory developed in this section was subjected to experimental verification. Several of the parameters in Eq. 2 were varied to determine the effect on the phase shift. Sensitivity measurements were also taken and compared with the theoretical sensitivity. The experimental setup and results are discussed in detail in the next chapter.

2.2 The Michelson Interferometer

Previous work has been aimed at investigating the Michelson interferometer and the mathematically equivalent Mach-Zender interferometer.[1] In both of these configurations, the laser beam is split into two beams. One beam passes through the acoustic field and is called the sensing leg, while the other beam is isolated from the acoustic field and is called the reference leg. Only the sensing leg is modulated by the acoustic pressure. The phase difference between the two legs is given by

$$\Delta\phi = k\ell \frac{\partial n}{\partial p} \Delta p$$

$$= \frac{k\ell(n-1)}{\rho c_s^2} p_o \sin t$$

Using this expression and the previous analysis concerning the theoretical signal to noise ratio, we can calculate the shot noise limit of the Michelson interferometer. We get

$$p_o = \frac{\lambda_o \rho c_s^2}{\pi \ell (n-1)} \sqrt{\frac{2h\nu\Delta F}{\eta P_o}}$$

One of the problems encountered with the Michelson interferometer is unwanted phase distrubances between the reference and sensing legs. These disturbances can be introduced by mechanical vibrations other than acoustic vibrations which affect the two legs differently. They can also be introduced by temperature or pressure changes in the media carrying the light. However, these changes do not occur at normal acoustic frequencies, and will only cause the problem of shifting the fringe pattern on the detector which could make detection of the acoustic modulation difficult. As mentioned earlier, a $\pi/2$ phase shift between the beams is necessary to provide maximum sensitivity, and temperature and pressure effects can make this difficult to maintain.

It was suggested by R. A. Smith[2] that optical fibers containing the reference and sensing beams of the interferometer could be environmentally coupled while still isolating the reference beam from the acoustic pressure. This can be accomplished by inserting the fibers into oversized tubing. One tube will be filled with air so as to isolate the fiber from acoustic pressures but thermally couple it with the surrounding environment, while the other tube will be filled with water so as to thermally and barometrically couple the fiber with the environment. Thus, the fibers will experience similar temperature variations, but only one will sense the acoustic field. This will make the alignment of the recombined beams more stable.

This still leaves vibrational problems between the fiber ends, collimating lenses, and beam splitter, but this is not a bad problem if everything is mounted solidly on a common base. Vibrational problems between the optical table and tank wall have caused problems in the past, but this may be alleviated by coupling both fibers to the tank with the tubing.

2.3 The Fabry-Perot Interferometer

A third kind of interferometer which might be very effective in detecting sound is the Fabry-Perot interferometer. It would be constructed out of a single-mode optical fiber with high-reflectance coatings deposited on the fiber ends. This interferometer has the advantages of high sensitivity per unit fiber length and good optical stability. It has the disadvantage that the fiber length is strictly limited by the coherence length of the laser light.

A Fabry-Perot etalon consists of two highly reflecting surfaces (either plane or curved), aligned to a common axis. The beam makes multiple reflections within the etalon, which interfere either constructively or destructively. The transittance of the etalon is then a function of the optical path length within the etalon. If the intensity reflectance at each surface is given by R, and the intensity transmittance at each surface is given by T, then the ratio of the intensity transmitted through the etalon to the incident intensity is[3]

$$\frac{I_t}{I_o} = \left(\frac{T}{1-R}\right)^2 \frac{1}{1 + \left(\frac{4R}{1-R}\right)^2 \sin^2\left(\frac{\delta}{2}\right)} \qquad (6)$$

where

$\delta = 4\pi n\ell/\lambda_o$

n = index of refraction

ℓ = fiber length

If the etalon is constructed from an optical fiber which is placed in an acoustic field, the index of refraction and the length of the fiber will be modulated by the acoustic pressure. Both of these effects work together to modulate δ, but the phase modulation due to the index change is much greater than the modulation due to the length change, so we will neglect the length change. The change in index of refraction is given by

$$\Delta n = \frac{\partial n}{\partial p} p_o \sin\Omega t$$

where

p_o = peak acoustic pressure

Ω = acoustic frequency

The effect of modulating δ on the transmitted intensity can be seen by looking at Figure 5. The phase δ will be modulated by an amount much less than the free spectral range. It is apparent then, that δ must be

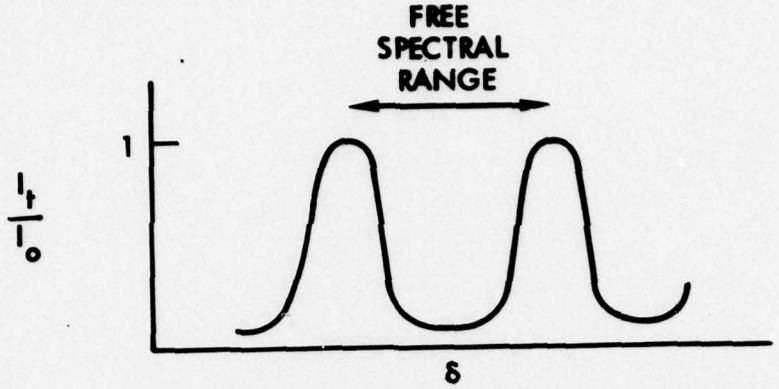

Figure 5. Transmittance vs phase in a Fabry-Perot

tuned near a peak so that I_t will change appreciably as δ changes. This tuning can be accompiished by running the fiber thorugh a small water-filled pressure chamber which can be varied over about one atmosphere. This will allow δ to be tuned to a point of maximum slope on Figure 5.

To understand the advantages of the Fabry-Perot interferometer, let us compare its response to the responses of the Michelson and differential interferometers. Since both the Michelson and differential interferometers are two-beam interferometers, their intensity vs phase curves are sine waves. The intensity vs phase curve for the Fabry-Perot is the Airy function given in Equation 6.

The phase modulation for each of the three configurations is shown in Table 1. Note that the Michelson and Fabry-Perot configurations have nearly equal phase modulations, while in the differential configuration the phase modulation is reduced by the factor Ω/c, where Ω is the acoustic frequency and c is the speed of light.

Table 1. A comparison of phase modulations

Michelson	$\Delta\phi = k\ell \frac{\partial n}{\partial p} p_o$
Differential	$\Delta\phi = \frac{8\Omega k}{c} \ell_1 \ell_2 \frac{\partial n}{\partial p} p_o$
Fabry-Perot	$\Delta\phi = 2k\ell \frac{\partial n}{\partial p} p_o$

The detector response under each of the configurations can be seen from Figure 6. In each case the intensity modulation is proportional to the phase modulation, but in the case of the Fabry-Perot, the proportionality constant is much higher if the finesse is large. For a finesse of 300 (corresponding to a reflectance of 99%) the proportionality constant is 100. The proportionality constant in the case of the Michelson and differential interferometers is one. Thus, with comparable fiber lengths, the Fabry-Perot can be made 100 times more sensitive than the Michelson, and thousands of times more sensitive than the differential at low acoustic frequencies. The shot noise limited sensitivies are compared in Table 2.

Another advantage of the Fabry-Perot is that its optical stability is as great as that of the differential interferometer, since all beams are contained in the same fiber.

One disadvantage is that the length of the fiber is limited by the coherence length of the laser employed. In fact, the coherence length of the laser must be many times longer than the fiber length if a large number of beams are to interfere with one another. This problem is serious enough so that the Michelson interferometer is still probably the best choice if long fibers are to be employed.

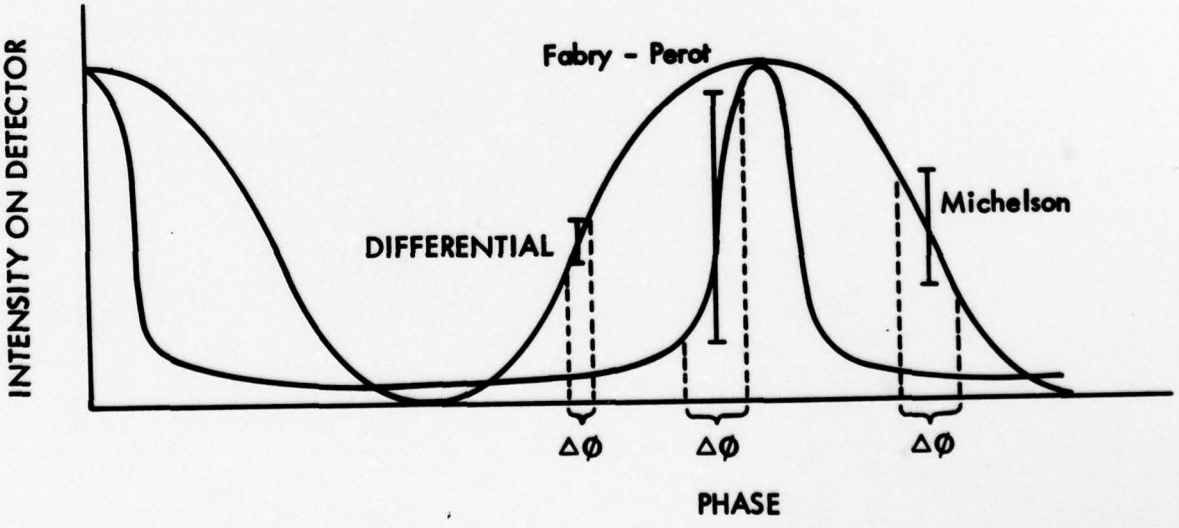

Figure 6. A comparison of the Michelson, differential, and Fabry-Perot responses to identical acoustic fields. (The $\Delta\phi$'s are exaggerated considerably.)

Table 2. A comparison of the theoretical sensitivities of three acousto-optic interferometers.

Parameters

$\ell = \ell_1 = \ell_2 = 30$ cm

$P_o = 300$ mW

$\eta = .3$

$\lambda_o = 514$ nm

$n = 1.5$

$\Omega = 10$ kHz

$\Delta F = 1$ Hz

$R = 99\%$

Interferometer	Shot noise limit	
Differential	$\frac{\lambda_o c \rho c_s^2}{\pi \Omega \ell_1 \ell_2 (n-1)} \sqrt{\frac{2h\nu\Delta F}{\eta P_o}}$	47 db re 1 μbar
Michelson	$\frac{\lambda_o \rho c_s^2}{\pi \ell (n-1)} \sqrt{\frac{2h\nu\Delta F}{\eta P_o}}$	-53 db re 1 μbar
Fabry-Perot	$\frac{(1-R)^2}{T} \frac{\lambda_o \rho c_s^2}{\pi \ell (n-1)} \sqrt{\frac{2h\nu\Delta F}{\eta P_o}}$	-87 db re 1 μbar

3.0 EXPERIMENTAL RESULTS

3.1 Large Tank Experiments with the Differential Interferometer

The experimental configuration used to test the differential interferometer is shown in Figure 7. A Lexel Model 85 argon-ion laser with a stabilized cavity was used as the light source. The first series of tests did not use an optical fiber, but rather used the raw laser beam guided by mirrors. The tank was constructed of Plexiglass and measured 19"x20"x16" deep. Two-inch thick hard rubber was used at the end of the tank to absorb the acoustic waves, but this later proved to be ineffectual at the frequencies we used.

The detector was a silicon photodiode which was wired across a 100 KΩ load resistor with no applied bias voltage. The detector signal was amplified by a PAR lock-in amplifier, consisting of a tuned amplifier followed by a phase-sensitive mixer and low-pass filter.

The acoustic pressure was measured with an NRL/USRD Type F-50 calibrated hydrophone. The hydrophone output was also measured with the PAR lock-in amplifier because of the electromagnetic interference which the hydrophone cable picked up.

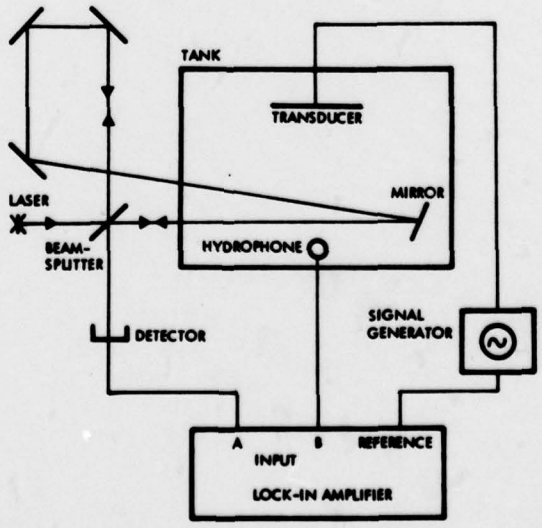

Figure 7. A schematic of the experiment.

The sensitivity of the differential interferometer was measured by decreasing the acoustic pressure in the tank until the signal from the detector could just be seen through the lock-in amplifier. The data are shown in Figures 8 and 9. Three things should be noted in particular. First, the theoretical sensitivity limit (limited by shot noise in this case) was not achieved. Second, the sensitivity did not improve significantly with increasing frequency as was expected. Third, the sensitivity did improve with increased path length in the delay leg.

The first two effects are primarily the result of the same problem, namely the curvature of the acoustic wavefront. The acoustic pressure along the laser beam was created by the superposition of many reflected sound waves, each of which had a curved wavefront. Thus, the index of refraction of the water was not modulated uniformly along the length of the laser beam, which means that only a portion of the interaction length was actually contributing to the phase shift of the light. This effective interaction length is reduced as the acoustic wavelength decreases, which accounts for the flat frequency response.

The decrease in sensitivity at 20 kHz has not been completely understood, but is apparently an electrical problem and not an acoustic resonance in the tank as was first suspected, since it appeared again when using a different size tank.

3.2 Small Tank Experiments with the Differential Interferometer

In an effort to get a plane acoustic wavefront, we first tried to reduce the reflections in the large tank. The rubber slab we were using had very little effect, so we tried lining the tank with bricks that had holes drilled in them. This also had very little effect. The acoustic pressure did not decrease with distance from the transducer, indicating that there were a large number of reflected waves in the tank.

It was then decided that a much narrower tank would confine the acoustic waves to produce a better plane wave. This tank measured 5-1/2" wide by 16" long by 6" deep. The transducer was placed at one end and the laser beam directed through the tank near the other end. Sensitivity measurements were taken, and the data is shown in Figure 10. This time the theoretical shot noise limit was achieved. The sensitivity also improved with increasing frequency, although there was some small problem in the vicinity of 20 kHz.

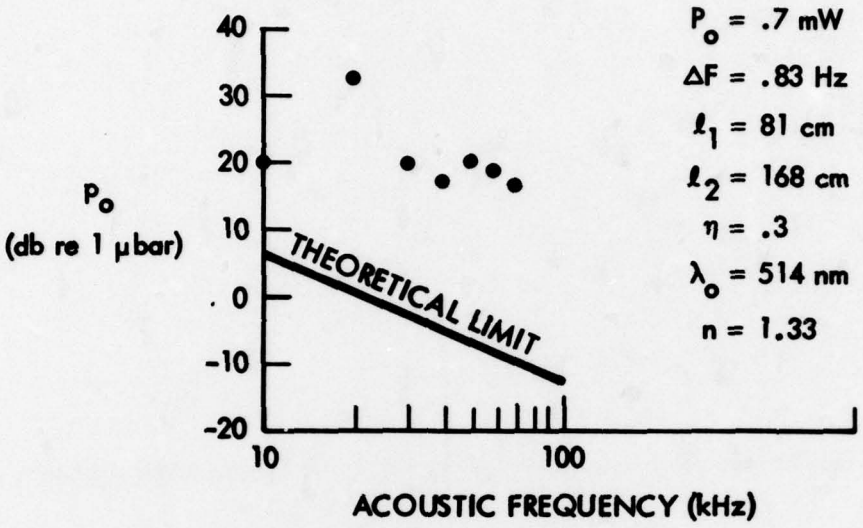

Figure 8. Sensitivity measurements of the differential interferometer with a short delay leg.

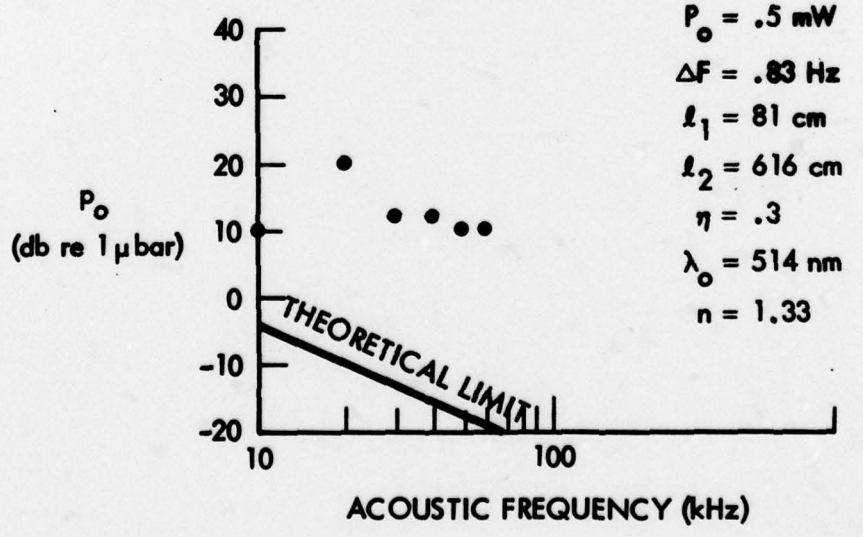

Figure 9. Sensitivity measurements of the differential interferometer with a long delay leg.

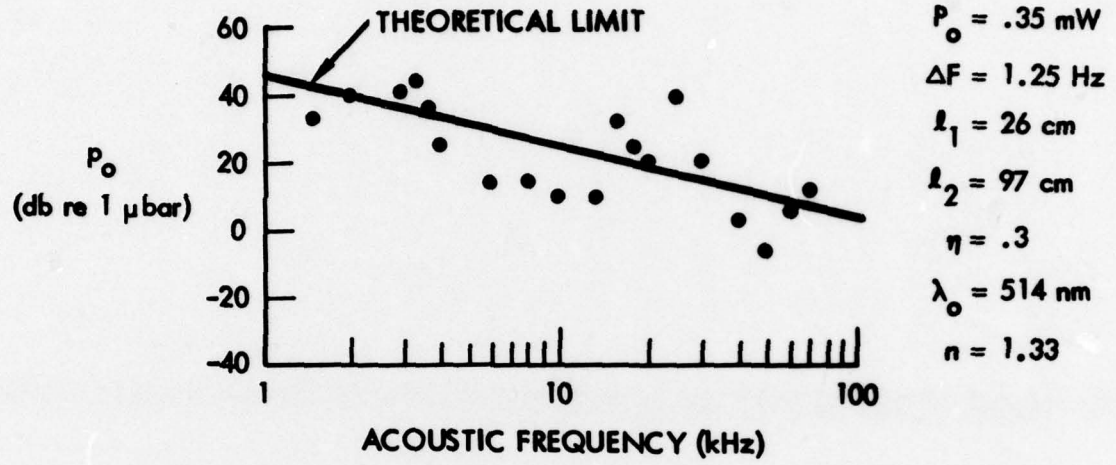

Figure 10. Sensitivity measurements of the differential interferometer using the small tank.

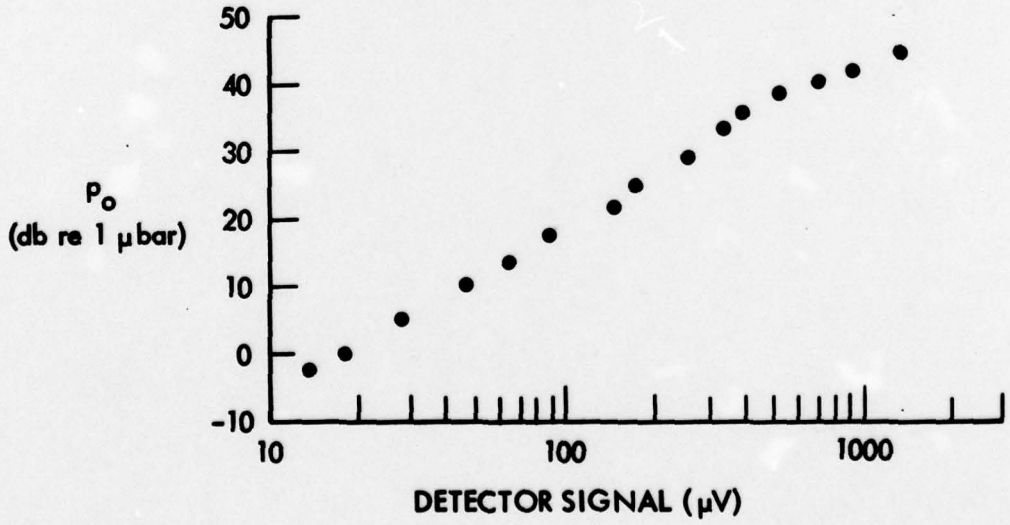

Figure 11. Response of the differential interferometer to loud acoustic fields.

It was also determined that a piezoelectric transducer placed in the tank as a receiver absorbed an appreciable amount of the acoustic energy falling on it and could be used to reduce reflections in the tank. With this transducer in the end of the tank, the readings from the calibrated hydrophone were much more stable at low sound levels. This indicates that there was a reduction of resonance effects in the tank.

The response of the differential interferometer to high acoustic pressures was also measured, as shown in Figure 11. The detector output is nearly linear with pressure, with the deviations caused partly by drifts in the laser power and partly by uncertainties associated with the measurements.

3.3 Experimental Efforts with the Michelson Interferometer

The Michelson interferometer was tested with fibers placed in oversized tubing. We were unable to achieve the shot noise limit with our apparatus, primarily because of difficulties in coupling light into the core of the fiber.

The fiber was a single-mode glass fiber purchased from ITT. The cladding was 80 microns in diameter with a 4.5 micron core. The fiber was covered with layers of plastic which made the fiber very easy to handle without breakage.

The tubing we used was round stainless steel tubing with an outside diameter of .040 inches and an inside diameter of .030 inches. Smaller tubing is readily available, but the plastic must be stripped from the fiber in order to fit it into smaller tubing. This makes the fiber more difficult to handle, as it tends to break easily when stripped.

It was necessary to strip the ends of the fibers in order to get them in the mounts, and also to couple the light out of the cladding, as will be explained in the next paragraph. The outer layer of plastic was melted off by dragging the fiber across a hot soldering iron. The inner layer did not melt off, but could be peeled off with the fingernails if one was careful. Some breakage did result from this technique, but it was found to be faster than using acid as had been done previously.

Only that portion of the light that is focussed into the fiber core will propagate as single-mode radiation. Any light that is focussed into the cladding will propagate in a multimode fashion, which is unsuitable for interferometry. Multimode radiation has essentially a random phase distribution over any cross section of the beam. In order to get rid of the multimode radiation in the cladding, a few drops of glycerin were placed on the fiber which was then sandwiched between two glass plates. This caused much of the light in the cladding to be lost into the glass plates, so that most of the light getting through the fiber was single mode.

Sensitivity measurements were performed using the Mach-Zender configuration shown in Figure 12. The analysis of the Michelson interferometer is completely applicable here since the only difference between the Michelson and Mach-Zender is the number of times the light traverses each leg. In a true Michelson interferometer, the path length is twice the physical length of the leg.

Measurements were first taken with the reference fiber enclosed in air-filled tubing and looped down into the tank alongside the sensing fiber, which was not enclosed in tubing. The data taken at two different times is

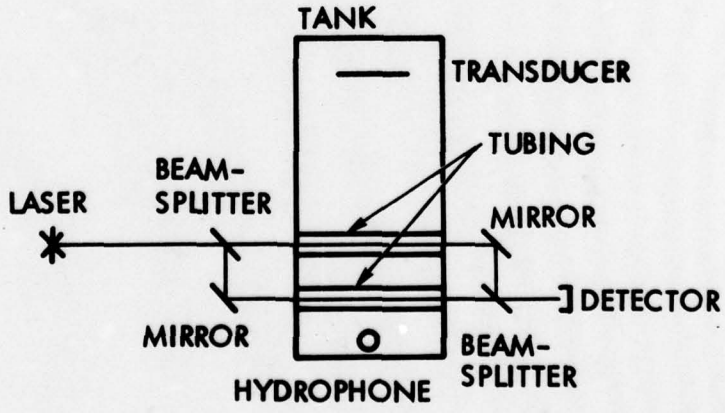

Figure 12. A schematic of the Mach-Zender configuration.

shown in Figure 13. Note that the shot noise limit was not achieved at any frequency. Also note that although the theory predicts a flat frequency response, there were definite peaks and dips in the curve. It is not known at the present time whether this was caused by resonances in the tank or peculiarities in the detector-amplifier system.* The most probable reason the shot noise limit was not achieved is that much of the radiation coming out of the fibers was multimode, even after mode stripping with the glycerin and glass plates. Fringes were just barely discernible even with careful alignment.

The Mach-Zender interferometer was also tested with both fibers enclosed in tubing. One tube was air filled to isolate the fiber from the acoustic field while the other was water filled to couple the fiber to the acoustic field. The detector output is shown as a function of acoustic pressure in Figure 14. The curve is roughly linear as expected. However, the detector output was not really very stable. The lock-in amplifier reading wavered between the positive and negative sides of the scale, indicating difficulties in matching the detector signal to the reference signal. The weakness of the detector signal is possibly because of the low light level of the single-mode radiation or because of poor coupling between the sensing fiber and acoustic field. Stainless steel is not very well matched acoustically to water, so there may have been some trouble in transmitting the sound wave through the tubing to the fiber. It is thought that the small diameter and thin wall of the tubing would allow good acoustic coupling, but more work must be done to see if this is really so.

*From private communication with J. H. Cole at the Naval Research Laboratory, it was learned that the Lexel laser is noisy, particularly at low frequencies, and probably contributed to our poor sensitivity.

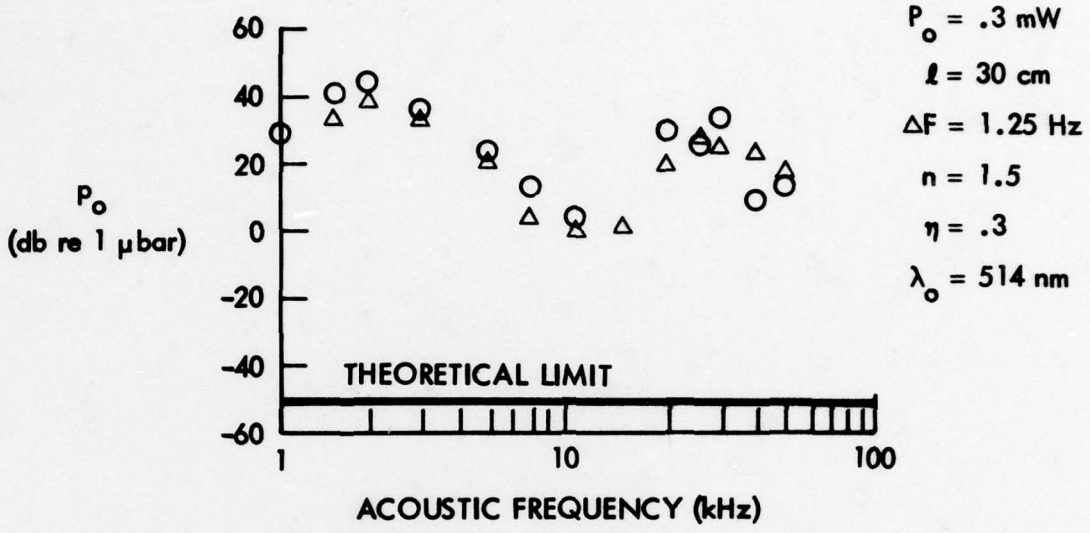

Figure 13. Sensitivity measurements of the Mach-Zender interferometer with the reference leg enclosed in tubing.

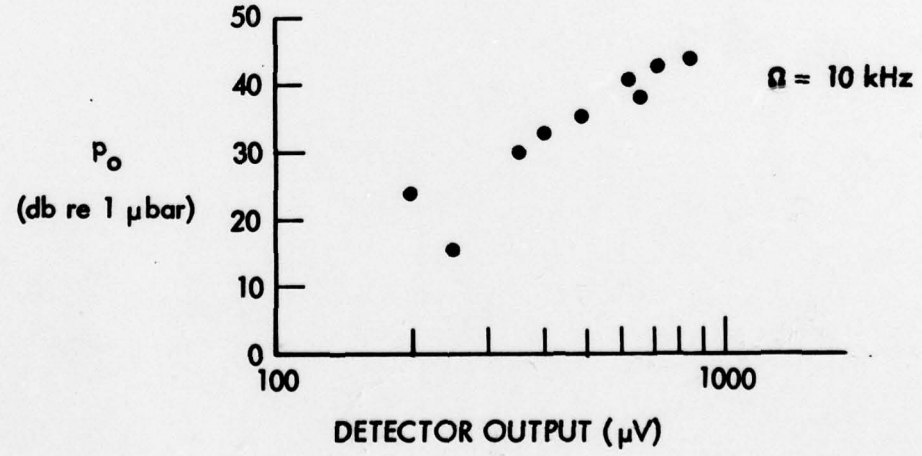

Figure 14. Response of the Mach-Zender interferometer with both legs enclosed in tubing.

4.0 CONCLUSIONS AND RECOMMENDATIONS

The theory underlying the fiber optic sonar system has been generally well supported by our data, although the theoretical limits have not been attained in all cases. The differential interferometer was shown to have good optical stability and low noise, and did respond at the theoretical limit of sensitivity. The Mach-Zender interferometer did not respond at the theoretical limit of sensitivity, but the idea of environmentally coupled fibers was shown to be workable. Many of the problems with the Mach-Zender are understood and can certainly be resolved with additional work. The Fabry=Perot interferometer was analyzed and shown to be very sensitive, although the fiber length is rather severely limited.

The biggest difficulty encountered with the Mach-Zender interferometer was focussing light into the core of the fiber. Although it is theoretically possible to focus laser light to a spot size of a few wavelengths, this cannot be done without considerable care in designing the optics. Ideally the spot size should be roughly the same as the diameter of the fiber core, so that with proper alignment much light would enter the core. The fiber would have to be located right at the beam waist where the radiation wavefront is plane, because of the small acceptance angle of a fiber. Irregularities in the wavefront produced by the optical elements could drastically affect the amount of light injected into the fiber core. Additional work should be done in designing or locating a good lens system to couple light into single-mode optical fibers.

The overall stability of acousto-optic interferometers is not as good as it should be. The measurements were not always repeatable, since the interferometer seemed to be noisier at some times than others. Part of the problem was electromagnetic interference, which can be reduced by proper shielding. It is also possible that temperature drifts caused the interferometer to go in and out of alignment, making consistent measurements difficult. If this is the case, the method of environmentally coupling the fibers with tubing should be of help. The alignment of any interferometer is critical, so to provide maximum stability thermal controls must be incorporated into the system.

Another problem that one should be aware of is with the reference signal that was fed into the lock-in amplifier. In an actual sonar system, no reference signal would be available other than the internal signal. It was more difficult to get a reading with an internal reference than with an external reference taken from the source. However, in actual use the sounds would not be nearly so pure in frequency as in the laboratory, and detection with an internal reference signal would be easier with broad band acoustic sources than with narrow band sources. Thus, in actual use the internal reference should work well, but it would be wise to check this out with a broadband source in the laboratory.

Theoretical sensitivities as a function of fiber length are shown in Figure 15. The improvement of the differential interferometer with fiber length is greater than that of the other interferometers because of its dependence on the lengths of both the sensing and time-delay legs. The approximations used in analyzing the differential interferometer are not valid for extremely long fiber lengths, so that extrapolation beyond 1 Km will not be linear.

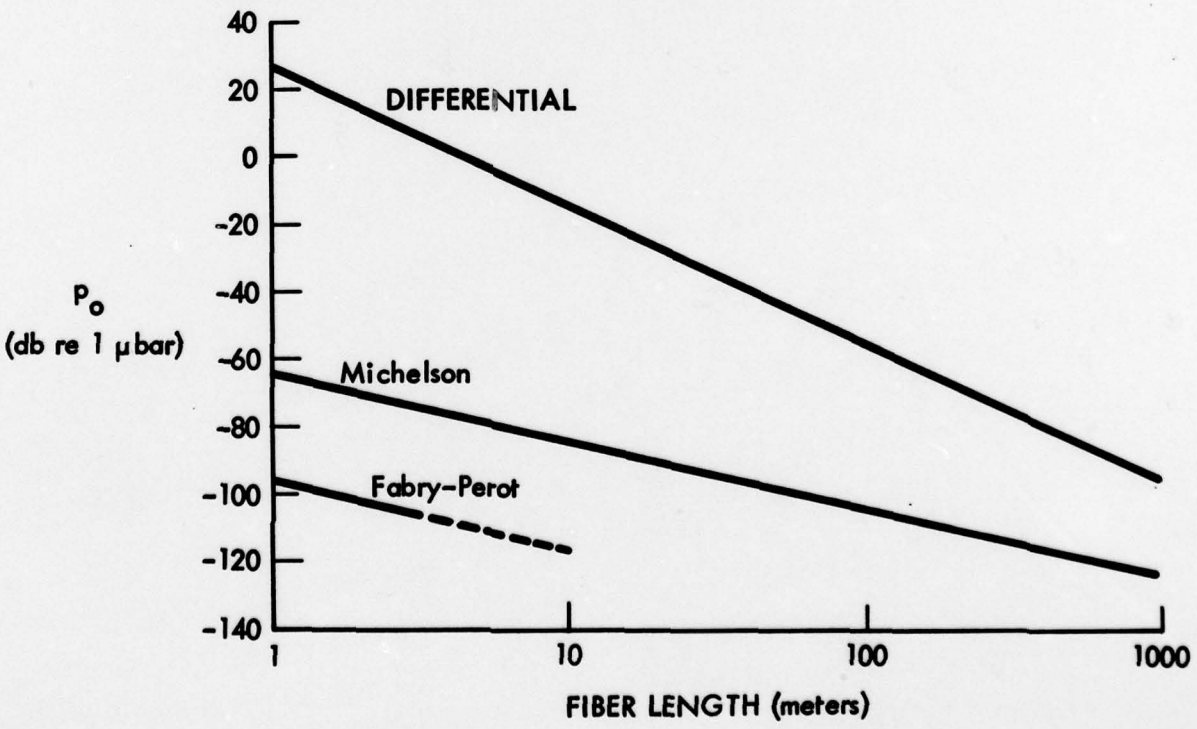

Figure 15. Extrapolation of theoretical sensitivities to long fiber lengths, using the parameters of Table 2.

It was apparent when taking data that noise and instability problems were worse at lower acoustic frequencies, particularly below 10 KHz. Although there was a definite response to acoustic fields down to 1 KHz, the response wavered more and appeared generally more unstable. Several things were contributing to this difficulty. First, it was noticed that there was considerable low frequency noise from the detector when the unmodulated laser beam was incident on the detector. It is not yet clear whether this problem arises from the laser, the detector, or the amplifier, but all should be viewed with suspicion. Also, as discussed earlier, acoustic reflections in the tank cause problems. Since the acoustic wavelength is comparable with the tank dimensions at low frequencies, standing waves tend to get set up instead of traveling waves. Even the calibrated piezoelectric hydrophone gave unstable, inconsistent results under low-frequency, low-pressure conditions. A very long, moderately wide tank would be best for low frequency measurements, although it becomes difficult to isolate the fibers from tank wall vibrations and the tank wall from ground vibrations. Hanging the fibers into the tank from a vibration-free granite table would help in reducing noise. A third difficulty with low frequency measurements is that 1/f noise becomes a problem. Usually it is larger than shot noise only at frequencies below 1 KHz, but it is sometimes a problem above this frequency.

Our overall conclusion is that the fiber optic sonar system is well worth pursuing, but that it needs much more development to overcome noise and stability problems. The construction of a practical system probably awaits further development of integrated optics. Beam-forming applications require the switching of light from fiber to fiber, which could be done quickly and compactly with integrated optics. An integrated optics package would also be free from alignment difficulties under field conditions, making its use on board vessels more feasible.

5.0 REFERENCES

1. J. H. Cole, R. L. Johnson and P. G. Bhuta, "Feasibility Demonstration of Fiber Optic Detection of Low Frequency Sound," TRW Report AT-ATD-TR-78-3, 31 July 1978, Page 16.

2. R. A. Smith, TRW Defense and Space Systems Group, Redondo Beach, CA; Private communication.

3. Hecht and Zajac, Optics (Addison-Wesley Publishing Company, 1974), page 308.

DISTRIBUTION LIST

	No. of Copies
Office of Naval Research Department of the Navy Arlington, VA 22217	
Attn: Mr. R. G. Joiner, Code 465	1
Mr. R. F. Obrochta, Code 222	1
Mr. M. A. Blizard, Code 212	1
Admin. Contracting Officer, Code SO527A	1
Director, Naval Research Laboratory Department of the Navy Washington, D.C. 20375	
Attn: Mr. R. R. Rojas, Code 8101	1
Dr. J. A. Bucaro, Code 8133	1
Dr. C. M. Davis, Code 8130	1
Dr. T. G. Gallorenzi, Code 5570	1
Mr. J. N. Cole	1
Defense Documentation Center Building 5, Cameron Station Alexandria, Virginia 22314	12
Office of Naval Research Branch Office 1030 East Green Street Pasadena, CA 91106	1
Defense Advanced Research Projects Agency 1400 Wilson Boulevard Arlington, VA 22209	
Attn: LCDR Wesley Jordan	1
Capt. Harry V. Winsor	1
Dr. E. Blase	1
New London Laboratory Naval Underwater Systems Center New London, Connecticut 06320	
Attn: Mr. Milton Green, Code 313	1
Commander, Naval Ocean Systems Center Department of the Navy San Diego, CA 92132	
Attn: Mr. Harper Whitehouse	1
Department of the Navy Office of the Chief of Naval Operations Washington, D.C. 20350	
Attn: Dr. W. O. Mehuron	1
Department of the Navy Office of the Asst. Secretary of the Navy Washington, D.C. 20350	
Attn: Dr. Thomas Quinn, OASN R&D	1
Commander, Naval Sea Systems Command Department of the Navy Washington, D. C. 20362	
Attn: NAVSEA 03423 (Mr. F. J. Romano)	1
NAVSEA 06H1 (Mr. C. D. Smith)	1
Naval Electronic Systems Command Department of the Navy 2511 Jefferson Davis Highway Arlington, Virginia 20360	
Attn: Dr. George Hetland, Jr., PME 124-62	1
Mr. Douglas Gaarde, PME 124-624	1